

ETCE/OMAE2000-6125

NONLINEAR RANDOM OCEAN WAVES: PREDICTION AND COMPARISON WITH DATA

Alok K. Jha

Senior Engineer
Bechtel, 50 Beale Street
San Francisco, California 94105
Email: ajha12@yahoo.com

Steven R. Winterstein

Department of Civil & Env. Engr.
Stanford University
Stanford, California 94305-4020
Email: steve@ce.stanford.edu

ABSTRACT

Nonlinear hydrodynamic effects are of growing interest for ocean structures and vessels. This paper investigates one of the most fundamental nonlinearities in ocean engineering: the wave elevation at a fixed spatial location. Nonlinear ocean waves have been the subject of research for a number of years, but have not yet entered common ocean engineering practice. This is perhaps due to the cumbersome need for time-domain simulation of second-order waves, or to the lack of systematic comparison of these models with observed data. This paper seeks to address both these issues by (a) developing convenient analytic formulas for the statistics of second-order random waves, and (b) comparing predictions based on these formulas to data from wave tank tests and field observations.

Water-depth dependent analytic formulas have been developed to predict the skewness and kurtosis (the third and fourth moments, respectively) of nonlinear random waves as functions of parameters that characterize a steady-state "seastate." These seastate parameters include the significant wave height and the spectral peak period. Analytic formulas are also developed for predicting the wave elevation and crest heights with specified return periods using the Hermite model. These formulations are compared with second-order random wave simulations as confirmation of the analytic formulas.

The analytic formulas for skewness and kurtosis are compared with observed data to indicate the accuracy of the second-order predictions. The analytic predictions of the elevations, crest heights and wave heights are also compared to observed data to study their accuracy. Finally, a comparison of the local

wave properties from second-order wave simulations to the wave tank data is shown. These local wave properties include, for example, crest height given wave height, wave period given wave height and crest period given wave height. These may be of interest in understanding "ringing" (high frequency response) of tethered floating structures.

INTRODUCTION

Nonlinear hydrodynamic effects are of growing interest for ocean structures and vessels. Here we study such effects in one of the most fundamental nonlinearities in ocean engineering: the wave elevation $\eta(t)$ at a fixed spatial location.

It is common practice to model $\eta(t)$ using linear wave theory, which results in a Gaussian model of $\eta(t)$. This ignores the marked asymmetry in the waves: wave crests that systematically exceed their neighboring troughs. This asymmetry increases with decreasing water depth. This asymmetry has several practical implications; for example, (1) asymmetric waves are more likely to strike decks on offshore platforms, particularly older Gulf-of-Mexico structures designed with fairly low decks; and (2) unusually large dynamic structural responses have been found in high, steep waves that may not follow linear wave theory.

Second-order random wave models are not new; indeed, they have been a research topic for more than 30 years (e.g., Tick, 1959; Hasselmann, 1962; Longuet-Higgins, 1963; Sharma & Dean, 1979; Hudspeth & Chen, 1979; Tayfun, 1980; Anastasiou *et al.*, 1982; Huang *et al.*, 1983; Langley, 1987; Winterstein

et al., 1991) and remain so today (e.g., Marthinsen & Winterstein, 1992; Hu & Zhao, 1993; Vinje & Haver, 1994; Winterstein & Jha, 1995). However, they have not entered common offshore engineering practice, which applies either random linear (Gaussian) waves, or regular waves that fail to preserve $S_\eta(\omega)$, the wave power spectrum.

Several drawbacks to second-order random waves may be suggested: (1) convenient statistical analysis methods for second-order models are often lacking; and (2) the accuracy of second-order models may be questioned, for example due to their neglect of still higher-order effects. We seek to address both concerns here. Regarding the first issue, we fit new analytical results for wave moments, and establish moment-based estimates of the probability distributions of wave elevation, crests, and heights. The second issue, concerning accuracy of second-order models, is addressed through comparison of theory with various wave tank and ocean wave measurements.

WAVE MODEL

Second-order Volterra models [Schetzen, 1980] have come under increasing use for modeling non-Gaussian random processes in offshore engineering (e.g. Winterstein *et al.*, 1994b; SWIM 2.0, 1995; WAMIT 4.0, 1995). $\eta(t)$ is accordingly modeled as the sum of a linear (Gaussian) process $\eta_1(t)$ plus a second-order (non-Gaussian) correction, $\eta_2(t)$, which is found from a perturbation analysis:

$$\eta(t) = \eta_1(t) + \eta_2(t) \quad (1)$$

For the second-order $\eta(t)$ in Eqn. 1, the standard Fourier sum for the linear part $\eta_1(t)$ is

$$\eta_1(t) = \sum_{k=1}^N A_k \cos(\omega_k t + \theta_k) = \text{Re} \sum_{k=1}^N C_k \exp(i\omega_k t) \quad (2)$$

in which Re indicates the real part of a complex number, and $C_k = A_k \exp(i\theta_k)$ are the complex Fourier amplitudes, defined in terms of Rayleigh distributed amplitudes A_k , and uniformly distributed phases θ_k . The C_k 's are mutually independent of one another. The mean-square value of A_k is

$$E[A_k^2] = 2S_\eta(\omega_k)d\omega_k; \quad d\omega_k = \omega_k - \omega_{k-1} \quad (3)$$

Based on Volterra theory, second-order corrections are induced at the sums and differences of all wave frequencies contained in $\eta_1(t)$:

$$\eta_2(t) = \text{Re} \sum_{m=1}^N \sum_{n=1}^N C_m C_n \left[H_{mn}^+ e^{i(\omega_m + \omega_n)t} + H_{mn}^- e^{i(\omega_m - \omega_n)t} \right] \quad (4)$$

In general, the functions H_{mn}^+ and H_{mn}^- are known as quadratic transfer functions (QTFs), evaluated at the frequency pair (ω_m, ω_n) . Similar expressions arise in describing second-order diffraction loads of floating structures [Jha *et al.*, 1997]; in this case the QTFs are calculated numerically from nonlinear diffraction analysis (e.g., WAMIT 4.0, 1995).

In predicting motions of floating structures, in view of the relevant natural periods, interest commonly lies with either H_{mn}^+ (springing) or H_{mn}^- (slow-drift) but not both. For example, in the case of the spar floating structure [Jha *et al.*, 1997], the slow-drift forces and hence the difference-frequency components generally govern the global motions of the spar. In contrast, in the nonlinear wave problem both sum and difference frequency effects play a potentially significant role. Fortunately, unlike QTF values for wave loads on floating structures, which must be found numerically from diffraction analysis, closed-form expressions are available for both the sum- and difference-frequency QTFs for second-order waves (e.g., Langley, 1987; Marthinsen & Winterstein, 1992). Including the effect of a finite water depth d , for example, the sum-frequency QTF can be written as

$$H_{mn}^+ = \frac{\frac{gk_m k_n}{\omega_m \omega_n} - \frac{1}{2g}(\omega_m^2 + \omega_n^2 + \omega_m \omega_n) + \frac{g}{2} \frac{\omega_m k_n^2 + \omega_n k_m^2}{\omega_m \omega_n (\omega_m + \omega_n)}}{1 - g \frac{k_m + k_n}{(\omega_m + \omega_n)^2} \tanh(k_m + k_n)d} - \frac{gk_m k_n}{2\omega_m \omega_n} + \frac{1}{2g}(\omega_m^2 + \omega_n^2 + \omega_m \omega_n) \quad (5)$$

in which the wave numbers k_n are related to the frequencies ω_n by the linear dispersion relation $\omega_n^2 = gk_n \tanh(k_n d)$. The corresponding difference-frequency transfer function, H_{mn}^- , is found by replacing ω_n by $-\omega_n$ and k_n by $-k_n$.

Because $\eta(t)$ is non-Gaussian, interest focuses on its skewness α_3 and kurtosis α_4 . In terms of the significant wave height $H_s = 4\sigma_\eta$, and peak spectral period T_p , these are predicted by a second-order wave model to be of the form:

$$\alpha_3 \sigma_\eta^3 = \overline{(\eta_1 + \eta_2)^3} = m_{31}(T_p)H_s^4 + m_{33}(T_p)H_s^6 \quad (6)$$

$$(\alpha_4 - 3)\sigma_\eta^4 = \overline{(\eta_1 + \eta_2)^4} = m_{42}(T_p)H_s^6 + m_{44}(T_p)H_s^8 \quad (7)$$

(The overbars in these results denote the averaging or expected value operation.) The $m_{ij}(T_p)$ are ‘‘response moment influence coefficients,’’ the contribution to response moment (cumulant) i due to terms of order $O(\eta_2^j)$. In general these coefficients are conveniently calculated from Kac-Siegert analysis (Eqns. 12–15, Winterstein *et al.*, 1994b; Ude *et al.*, 1993). We assume here the spectrum of $\eta_1(t)$ is of the form $H_s^2 T_p f(\omega T_p)$, so that $\eta_1(t)$ scales in amplitude with H_s and in time with T_p . Such is the

form, for example, of a JONSWAP spectrum with fixed value of the peakedness parameter γ .

It is useful to define the unitless wave steepness $S_p = H_s/L_p$, in which the characteristic wave length $L_p = gT_p^2/2\pi$ uses the linear dispersion relation. Note that S_p is typically far less than unity, and a perturbation analysis commonly retains only leading-order terms in S_p . For deep-water waves the coefficients $m_{ij}(T_p)$ are proportional to L_p^{-j} , and they remain nearly so for finite depths as well. Retaining the leading terms in S_p from Eqns. 6–7:

$$\alpha_3 = k_3 S_p; \quad \alpha_4 - 3 = k_4 \alpha_3^2 \quad (8)$$

In particular, for a JONSWAP wave spectrum with peakedness factor γ , we have fit the following k_3 and k_4 expressions to results for a wide range of depths [Winterstein & Jha, 1995]:

$$k_3 = \frac{\alpha_3}{S_p} = 5.45\gamma^{-0.084} + \left\{ \exp \left[7.41 (d/L_p)^{1.22} \right] - 1 \right\}^{-1} \quad (9)$$

$$k_4 = \frac{\alpha_4 - 3}{\alpha_3^2} = 1.41\gamma^{-0.02} \quad (10)$$

The second term in this result for α_3 reflects the effect of a finite water depth d : in shallower waters the skewness α_3 grows, as the waves begin to “feel” the bottom.

Note also that while the skewness is predicted to vary linearly with steepness, the kurtosis is predicted from Eqn. 8 to vary quadratically with the steepness S_p . Since the steepness is far less than unity (squared steepness even smaller), this suggests that nonlinear effects will be most strongly displayed by the skewness, and hence by the wave crests rather than the total peak-to-trough wave heights. This second-order model may less accurately predict kurtosis, however, as higher-order omitted effects may be of the same order of magnitude.

Scope and Organization

In the following sections, we develop and compare analytical wave predictions to the second-order random wave model and to both wave tank data and ocean wave measurements. The comparisons are at the following three levels:

Moments of wave time histories: We will first compare the predicted wave history moments—specifically, the skewness, α_3 , and kurtosis, α_4 —across a broad range of seastates observed from both wave tank and measured ocean conditions.

Cumulative Distribution Functions (CDFs) of wave elevations, wave crests and wave heights: These comparisons will assess whether or not the second-order model is able to predict these CDFs, over and above predicting the third and fourth moments of the waves. Two distinct comparisons will be made: (1) analytical models of the various CDFs will be shown to accurately predict—and hence replace—the need for full time-domain simulation of random second-order waves; and (2) the resulting analytical models of the various CDFs will be used to assess the ability of second-order wave theory to predict wave elevations, crests, and heights in both wave tank and ocean field conditions.

Local Wave Parameters. This study investigates the ability of the model to predict local properties of the wave profile; e.g., marginal mean and standard deviation of a wave crest given a wave height, of wave period given a wave height and similar marginal moments of other local wave properties.

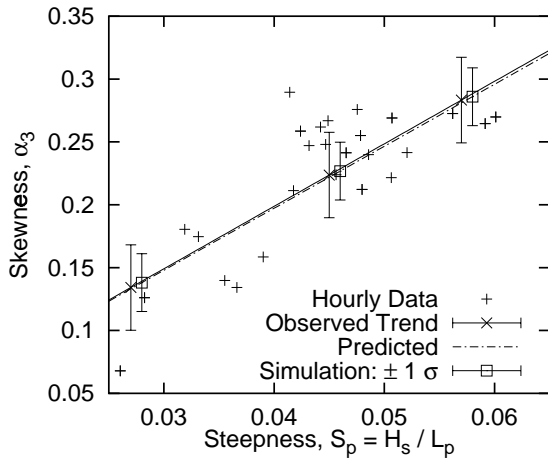
COMPARISON OF α_3 AND α_4 : DATA VS. PREDICTION

Here and throughout, we shall compare the predicted and observed wave results from two different data sets: one from a wave tank and one from the ocean. The wave tank measurements reflect wave histories with target H_s of 4m to 18m in approximately 308m water depth [MARINTEK, 1989; MARINTEK, 1990]. We consider 18 wave tank histories, each about 2 hours, processed here as 36 1-hour time histories. The ocean wave histories are laser measurements taken at the Ekofisk platform in the North Sea, located at a water depth of approximately 70m. These measurements are for durations of about 18 minutes, collected every 3 hours during the year 1984. From the annual data set, we select seastates with H_s above 4.5m and with skewness values between -0.05 and 0.4 (to avoid anomalous histories with potential measurement errors). This results in selection of 132 time histories.

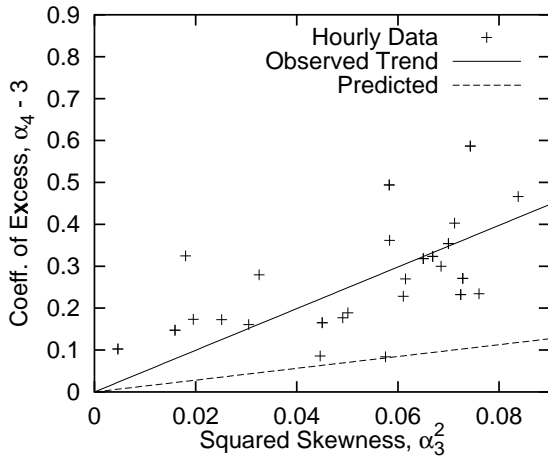
Figure 1 compares predicted skewness and kurtosis trends (from Eqns. 9 and 10 with $\gamma=3.3$) with the observed sample moments from the 1-hour wave tank histories. The predicted skewness trend line shows excellent agreement with the data: the predicted trend has slope $k_3=4.93$, compared with the slope estimate 4.97 ± 0.12 (mean \pm std. error) from the observed skewness values. Note that the effect of the depth-dependent ($d \approx 308$ m) term in Eqn. 9 will cause only a slight increase in the prediction and is neglected here.

In contrast, Fig. 1b shows that the second-order model considerably underestimates the kurtosis of the model test waves. The mean regression slope of 4.96 ± 0.33 for the observed k_4 is about 4 times the predicted k_4 value. This lends some support to the view, noted earlier, that the second-order model predicts the kurtosis value less accurately due to omitted higher-order effects [Vinje & Haver, 1994].

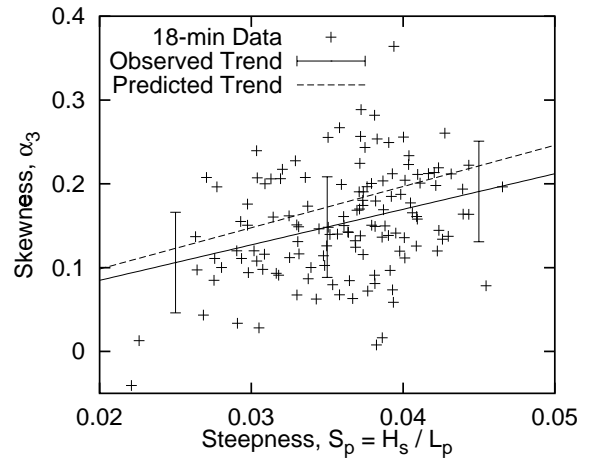
In contrast, for the Ekofisk field data, the second-order



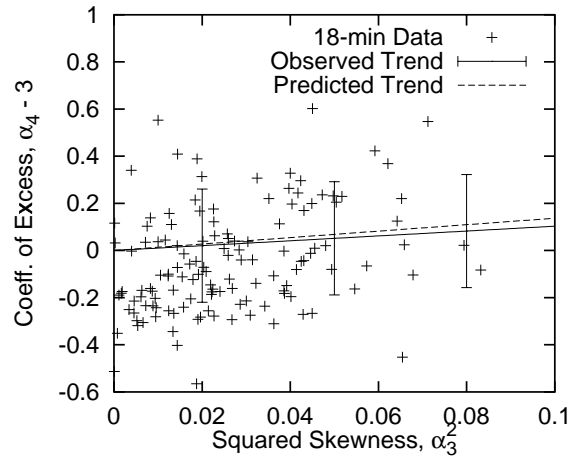
(a) Skewness comparison



(b) Kurtosis comparison



(a) Skewness comparison



(b) Kurtosis comparison

Figure 1. Skewness and kurtosis comparison for Snorre model test wave measurements and the second-order model

model is found to accurately predict *both* skewness and kurtosis. The predicted skewness is in fact a bit higher than measurements (Figure 2a), while the kurtosis prediction follows the observed trend almost exactly (Figure 2b). Note the additional scatter in observed skewness values compared with the preceding wave tank results; this arises because the Ekofisk samples are of only 20-minute durations. Note also that our “predicted trend” results are based on linear regression with zero intercept (i.e., constrained so that the Gaussian moments are obtained as the steepness S_p goes to zero).

In view of these results, one may ask why the second-order model should better match field data than model test results. Several possibilities may be advanced. First, the model test results may be indicative of more severe seastates, in which higher-order

Figure 2. Skewness and kurtosis comparison for Ekofisk ocean wave measurements and the second-order model using fitted H_s , T_p and γ values from measurements

effects (e.g., on kurtosis) may be more significant. Alternatively, the Ekofisk data may show short-crested behavior, which is not included in our long-crested second-order model. In this case, the apparent agreement between theory and model in Figure 2 may be the fortunate result of offsetting errors; i.e., while our model tends to underestimate nonlinear effects of long-crested waves, the short-crestedness of Ekofisk reduces the observed kurtosis values to a comparable level.

In any case, assuming the wave tank accurately reproduces severe seastates with long-crested waves, it appears that second-order models may underpredict nonlinear effects (e.g., kurtosis levels). The second-order model may be more adequate for more moderate conditions, as seen in Ekofisk.

Table 1. Summary information of the three wave data sets used in CDF comparisons of wave elevations, wave crests, and wave heights. H_s and T_p values are found from fitting a JONSWAP spectral shape, with $\gamma=3.3$ in all cases.

Set	Description	H_s (m)	T_p (s)	Duration (hrs)
1	Snorre: Tests 504,505,506	13.4	13.75	5.79
2	Snorre: Test 304	7.05	12.0	1.93
3	Ekofisk: 14 18-min segments	5.14	9.8	3.98

CDF PREDICTIONS I: ANALYTICAL VS SECOND-ORDER SIMULATION

As earlier noted, for practical applications we are concerned with the CDF (Cumulative Distribution Function) of various quantities; e.g., (1) the instantaneously varying wave elevation level; (2) the resulting wave crest height; and (3) the total crest-to-trough wave height. In this section, we propose a set of analytical models for each of these CDFs, and confirm that they adequately describe the simulated behavior of second-order random waves. This simplifies the application of second-order wave theory considerably, removing the need for full time-domain simulation of second-order waves (e.g., through double Fourier sums). The following section will then compare these simple analytical models—which are found consistent with second-order waves—with measured CDF results for both wave tank and Ekofisk field data.

Summary of Wave Case Studies

We focus here on three wave data sets: (1) three 2-hour measurements representing the same seastate from the Snorre wave tank tests, (2) one 2-hour measurement again from the Snorre wave tank tests, representing a less severe seastate with different steepness S_p , and (3) fourteen 18-minute Ekofisk wave measurements, chosen to represent similar climate conditions. We present a summary of the three data sets in Table 1.

Analytical Predictions for Second-order Simulations

The proposed analytical models to match the second-order simulated results are based on the Hermite model [Winterstein *et al.*, 1994a] for the wave elevation and crest height and based on the Naess model [Naess, 1985] for wave heights.

Analytical Wave Elevation Models. The Gaussian model for wave elevation is given as

$$\text{Prob}[\text{Elevation} > \eta] = 1 - \Phi\left[\frac{\eta - \bar{\eta}}{\sigma_\eta}\right] \quad (11)$$

where $\Phi()$ is the standard normal CDF, and $\bar{\eta}$ is the mean wave elevation. The Hermite model is in general a cubic transformation of a standard Gaussian process, based on the first four moments of the wave process. We use a simplified form of the Hermite model here, applicable over a wide probability range for second-order random waves. This simplification results because the predicted kurtosis levels for second-order waves do not significantly affect the transformations; hence, we only retain the quadratic, skewness-based term in the Hermite transformation. In this simplified Hermite model, a standard normal variable u can be transformed to a non-Gaussian wave elevation level x as follows:

$$x = g(u) = \bar{\eta} + \kappa\sigma_\eta\left[u + \frac{\alpha_3}{6}(u^2 - 1)\right] \quad (12)$$

where $\kappa = 1/\sqrt{1 + \alpha_3^2/18}$. For a given value of u , the transformed value $x = g(u)$ has the same CDF value of $\Phi(u)$. In practice, it is simplest to use this model by specifying a probability level p of interest: one first calculates the standard Gaussian fractile u_p (for which $\Phi(u_p) = p$), and substitutes that u value into Eqn. 12 to find the non-Gaussian fractile value. (Note that Eqn. 9 will be used here to predict the skewness value α_3 in Eqn. 12.)

Analytical Crest Height Models. The crest height of a Gaussian narrow-band process follows the Rayleigh distribution:

$$\text{Prob}[C_r > c] = \exp(-0.5(c/\sigma_\eta)^2) \quad (13)$$

The corresponding second-order crest elevation η_c at the same fractile can be estimated using the same transformation $g()$ as in Eqn. 12:

$$\eta_c = g(c_r) = \bar{\eta} + \kappa\sigma_\eta\left[c_r + \frac{\alpha_3}{6}(c_r^2 - 1)\right] \quad (14)$$

Again, one may first start with a given fractile c_p of the Rayleigh variable in Eqn. 13, and transform it to find the corresponding fractile of the non-Gaussian crest η_c .

Analytical Wave Height Models. For a narrow-band Gaussian process, the total crest-to-trough wave height also follows a Rayleigh model, with twice the amplitude of the crest

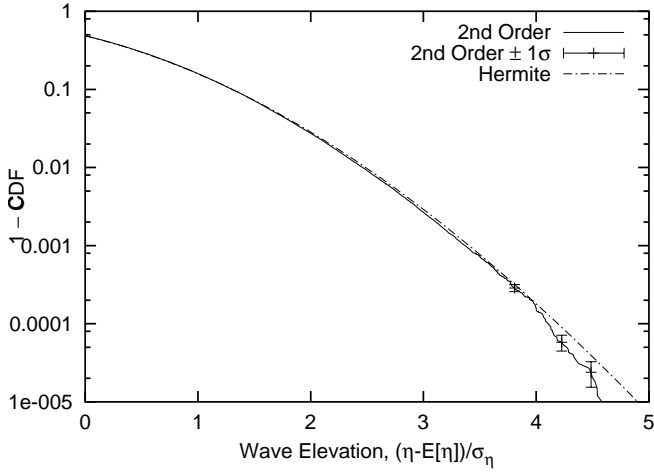


Figure 3. Wave elevation CDF: 2nd-order sim. vs. Hermite (Set 1)

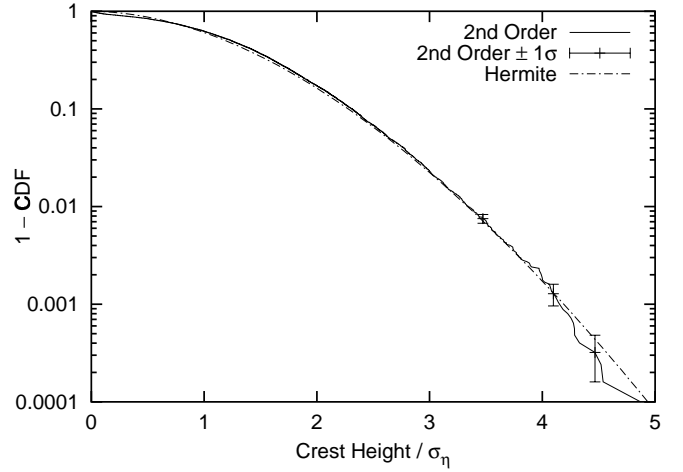


Figure 4. Norm. crest height CDF: 2nd-order sim. vs. Hermite (Set 1)

model in Eqn. 13:

$$\text{Prob}[H_r > h_r] = \exp\left[-\frac{(h_r/\sigma_\eta)^2}{8}\right] \quad (15)$$

For non-Gaussian processes, in contrast, positive skewness values indicate systematically larger crests than troughs, while larger-than-Gaussian kurtosis values (above 3) suggest systematic excess of the total crest-to-trough range (over that of a Gaussian process). As we have seen earlier, random second-order wave models have kurtosis values only slightly greater than 3; hence we may expect their predicted wave heights to be relatively unaffected by nonlinear effects.

The remaining correction to the Rayleigh model in Eqn. 15 concerns the effect of non-zero spectral bandwidth. Range values will tend to decrease, compared with the Rayleigh model, as the spectral bandwidth increases. We seek to reflect this effect through a simple model proposed by Naess:

$$\text{Prob}[H > h] = \exp\left[-\frac{(h/\sigma_\eta)^2}{4(1-\rho)}\right] \quad (16)$$

Here ρ is taken as the autocorrelation function value at half the dominant wave period. For a JONSWAP spectrum with $\gamma=3.3$ and 7.0 the values of ρ are -0.73 and -0.80 , respectively. Of course, as $\rho \rightarrow -1$ this result approaches the narrow-band Rayleigh model (Eqn. 15).

Numerical Results. The WAVEMAKER routine has been used here to simulate both first-order (Gaussian) and

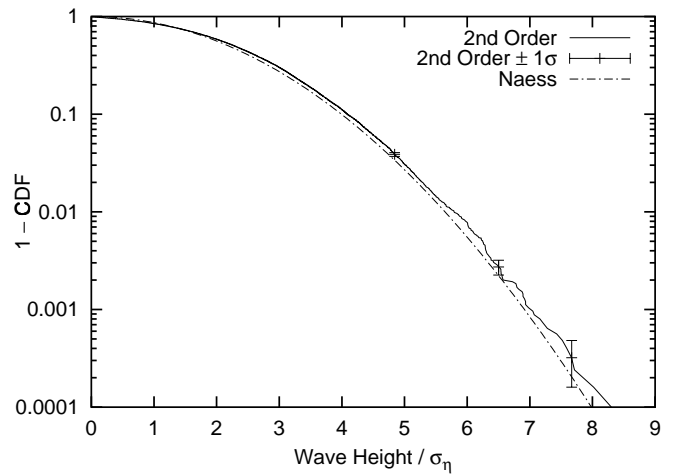


Figure 5. Norm. wave height CDF: 2nd-order sim. vs. Naess (Set 1)

second-order (non-Gaussian) wave time histories. These have been processed to develop the simulated CDFs of the wave elevations, crest heights and wave heights. Simulations have been performed for all three wave data sets. In each case, the simulations were based on the measured wave spectrum. The time resolution of the simulated histories is chosen to be the same as that of the measured histories ($dt=.42s$ for wave tank tests, $0.50s$ for Ekofisk). The total simulated durations are generally longer than the total observed durations, in an effort to “fill in” the tails of the distributions and thereby offer a more robust comparison in the tails.

The resulting CDFs for wave elevation, crest height, and wave height for data set 1 are shown in Figures 3, 4, and 5 re-

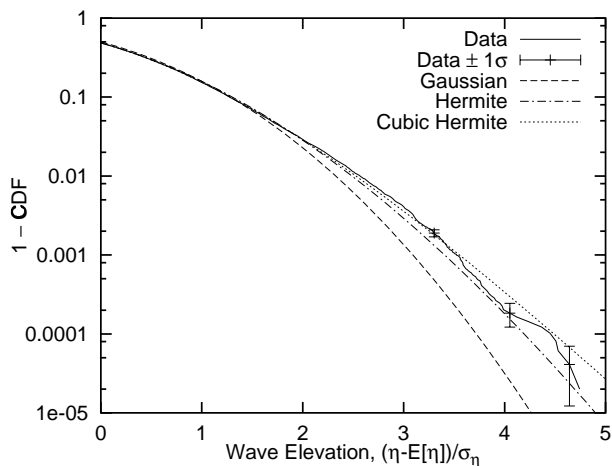


Figure 6. Wave elevation CDF: Data vs. analytical models (Set 1)

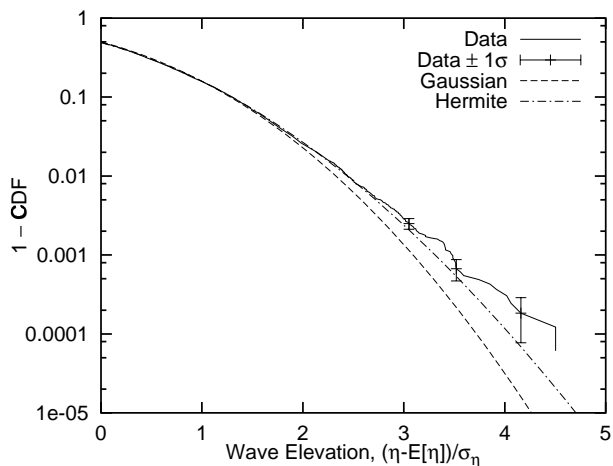


Figure 7. Wave elevation CDF: Data vs. analytical models (Set 2)

spectively. The analytical models are found to provide excellent agreement with the simulated second-order results. (The Naess model here uses $\rho = -0.73$ based on $\gamma = 3.3$). Similar levels of agreement were found for the remaining two data sets as well. Hence we believe these analytical models accurately represent the behavior of second-order random waves. They will be used in the next section to test whether this second-order random wave behavior is consistent with field and model test data.

CDF PREDICTIONS II: ANALYTICAL VS OBSERVATIONS

Comparison of Wave Elevation Distributions

The analytical models (for elevation, crest, and wave heights) are now compared here to the measured results from the three data sets. (Recall that these data sets are described in Table 1.) Figures 6, 7, and 8 show wave elevation CDFs for data sets 1, 2, and 3 respectively. In addition to the skewness-based Hermite model described above (Eqn. 12), Figure 6 also shows results for a model (“Cubic Hermite”) that uses all four wave moments, as obtained from the measured data. The standard Gaussian model is also included for comparison.

Results. As might be expected, the Gaussian model underestimates extreme wave elevations in all cases. With its inclusion of skewness effects, the Hermite model provides a notable improvement. This Hermite model is most accurate for the field data (set 3), while it somewhat underestimates wave elevations for the model test in data set 1 and (especially) in data set 2. (Note that this is not a deficiency of the Hermite model but rather of second-order wave theory, which has been used to parameterize the moment-based Hermite model.) This is not surprising, in

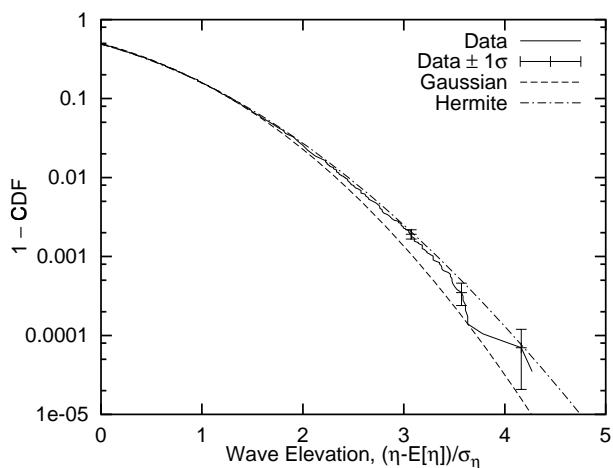


Figure 8. Wave elevation CDF: Data vs. analytical models (Set 3)

view of the earlier results showing that second-order models underestimated kurtosis values for wave tank histories (Figure 1b). Indeed, somewhat better agreement is found from the (Cubic) Hermite model, which is based on the actual four moments of the wave tank history (Figure 6).

Comparison of Crest Height Distributions

Figures 9, 10, and 11 show CDFs of wave crests for data sets 1, 2, and 3 respectively. In addition to the Hermite crest model (Eqn. 14), these figures show several other commonly used distributions. One is a Rayleigh model (Eqn. 13), consistent with a Gaussian model of the wave elevation process. Another is an

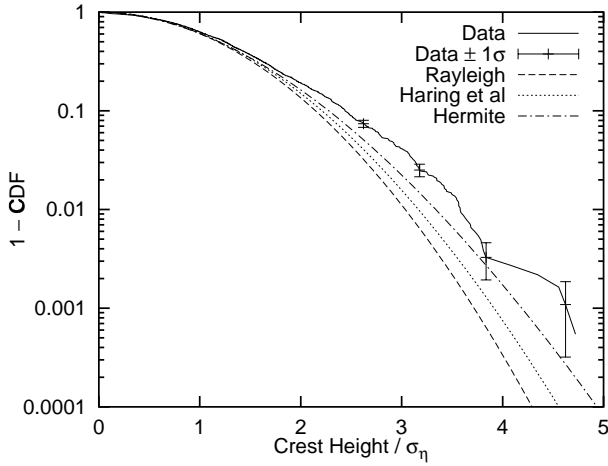


Figure 9. Norm. crest height CDF: Data vs. analytical models (Set 1)

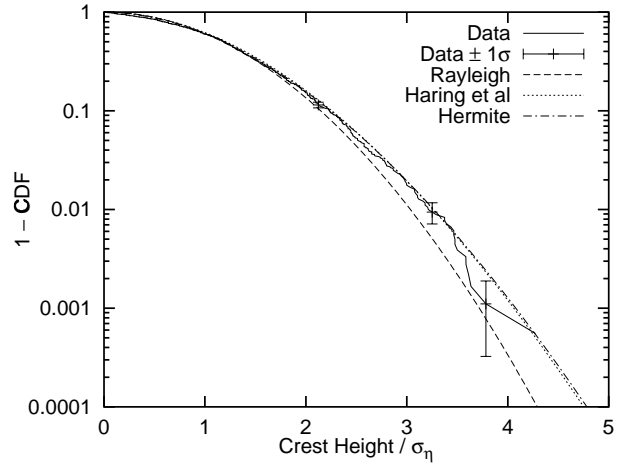


Figure 11. Norm. wave crest CDF: Data vs. analytical models (Set 3)

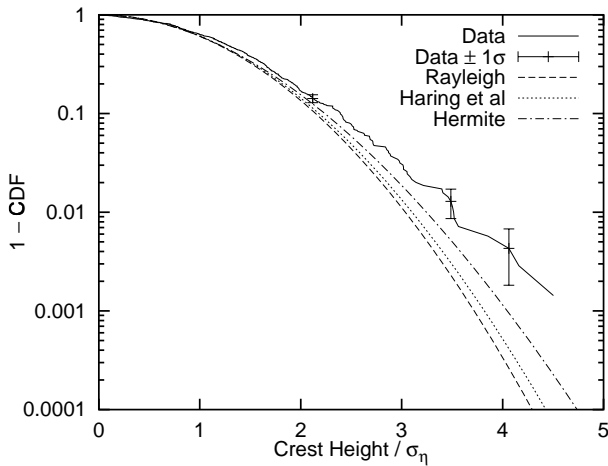


Figure 10. Norm. crest height CDF: Data vs. analytical models (Set 2)

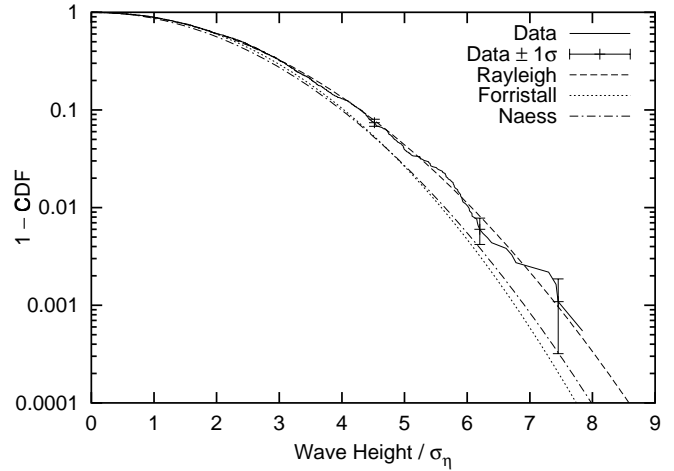


Figure 12. Norm. wave height CDF: Data vs. analytical models (Set 1)

empirical formula fit by Haring et al [Haring *et al.*, 1976] to observed ocean crest data:

$$\text{Prob}[C > c] = \exp \left\{ -\frac{1}{2} \left(\frac{c}{\sigma_\eta} \right)^2 \left[1 - 4.37 \frac{c}{d} \left(0.57 - \frac{c}{d} \right) \right] \right\} \quad (17)$$

Results. The crest CDFs show the same trends as the wave elevation results. The Rayleigh distribution, implied by a Gaussian process model, underestimates extreme crests in all cases. The Hermite model again provides an improvement, and is again most accurate for the field data (set 3). The Hermite

model (and hence second-order theory) underestimates extreme crests in the wave tank (Figures 9 and 10), to a greater degree than its underestimation of the wave elevation CDF. This again is consistent with the apparent kurtosis underestimation by second-order theory. Finally, the Haring model is roughly as accurate as the Hermite model for the field data (set 3; water depth $d=70\text{m}$), but is less accurate than the Hermite model for the wave tank tests (depth $d \approx 300\text{m}$). We believe the Haring model should not be applied, nor was intended to apply, in such deep-water locations; it was calibrated at shallower locations, and approaches the Rayleigh for deep-water sites.

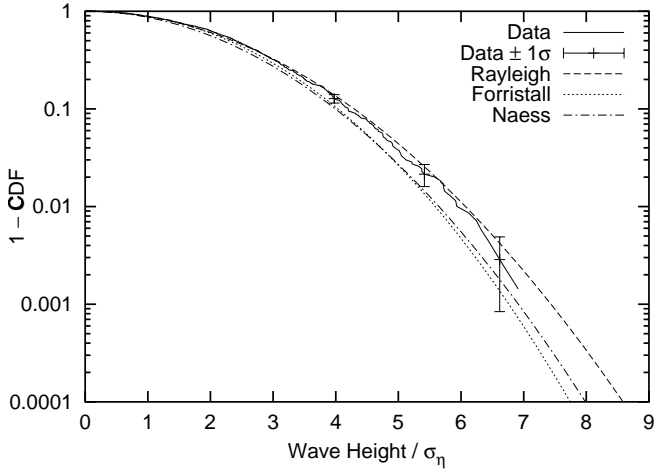


Figure 13. Norm. wave height CDF: Data vs. analytical models (Set 2)

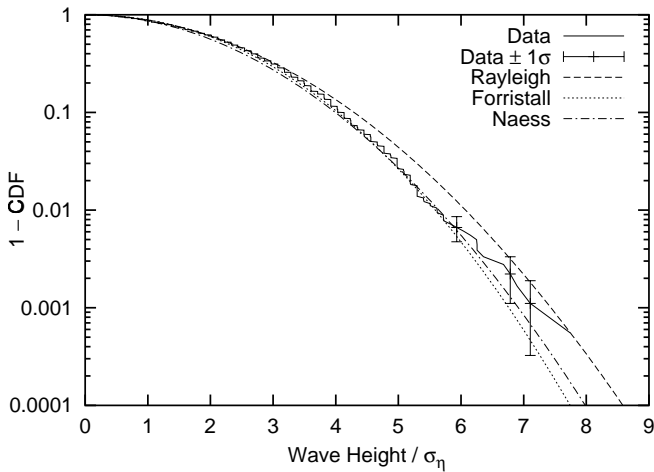


Figure 14. Norm. wave height CDF: Data vs. analytical models (Set 3)

Comparison of Wave Height Distributions

Finally, Figures 12, 13, and 14 compare observed wave height distributions with the Naess model, which was found an accurate proxy for second-order wave simulation. Also shown are a Rayleigh wave height model (Eqn. 15) and an empirical model suggested by Forristall [Forristall, 1978]. This Forristall model is a special case of a Weibull distribution, given as $\text{Prob}[\text{Height} > h] = \exp[-(h/\sigma_\eta)^{2.126}/8.42]$.

Results. Again, what is most notable in these results is the discrepancy between field and wave tank behavior. The second-order model and its analytical approximations (the Naess

model and, to a similar degree, the Forristall model) agree well with the field data. The wave tank data show larger wave heights than these models predict. This again would appear a direct consequence of the notably larger kurtosis of the wave tank histories: recall that kurtosis is expected to most directly impact peak-to-trough wave height. In fact, the simplest, Rayleigh model is found best able to match the wave tank results. This is likely a product of offsetting errors: the Rayleigh model neglects bandwidth effects that reduce wave heights (an effect captured by Naess and Forristall); however, the Rayleigh model (and others) neglect the high-kurtosis effect, which enhances the wave heights.

COMPARISON OF LOCAL WAVE STATISTICS

Finally, we compare the conditional distributions of various local wave parameters. The crest front period T_{CF} is the period from a mean-upcrossing to the time of occurrence of the highest point in a crest. The crest back period T_{CB} is similarly defined as the period between the highest point in a crest to the following mean-downcrossing. The crest period T_C is the sum of T_{CF} and T_{CB} and is the period between a mean-upcrossing and the following mean-downcrossing in the wave. The wave period T_W , finally, is the period between the two mean-upcrossings in a wave.

We will compare the conditional distribution of the local wave parameters from the second-order model to data. We will demonstrate these comparisons with the first wave data set that represents the Snorre wave tank measurements. We will first look at the conditional distribution of a wave's crest height given its wave height. Figure 15 shows the conditional mean and standard deviation of the wave crest given a wave height for the first- and second-order simulated histories and measured data. The Gaussian (first-order) simulation, of course, predicts that the crest heights are on average half the corresponding wave heights. The data shows systematically larger crests conditionally, given the corresponding wave height. The second-order model is found to predict this conditional vertical asymmetry quite accurately. Note that even though the model slightly underpredicts the marginal distributions of the crests and of the wave heights, the conditional crest mean and standard deviation seem accurately predicted.

We next consider the horizontal asymmetry in the waves. Figures 16 and 17 compare T_C to T_W , and T_{CF} to T_C , respectively. As may be expected, both the first-order and second-order simulations do not predict any horizontal asymmetry. As seen in the figures, T_C is approximately half of T_W . Similarly, T_{CF} is approximately half of T_C . No horizontal asymmetry can be found in the observed data either, indicating that the first- and second-order simulations are statistically similar to the observations as regards their horizontal symmetry.

Figure 18 shows the conditional distributions of wave peri-

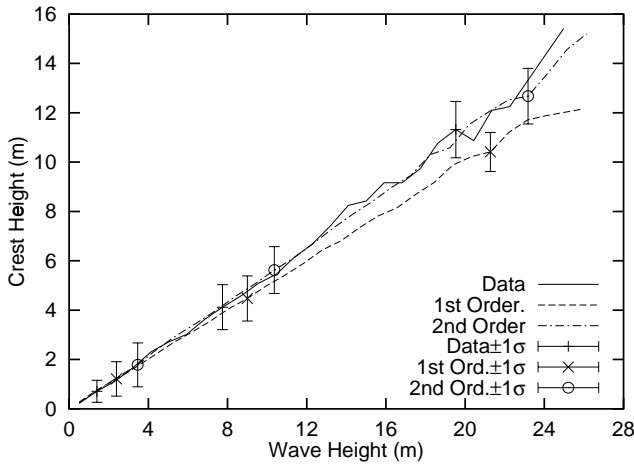


Figure 15. Crest height vs. wave height

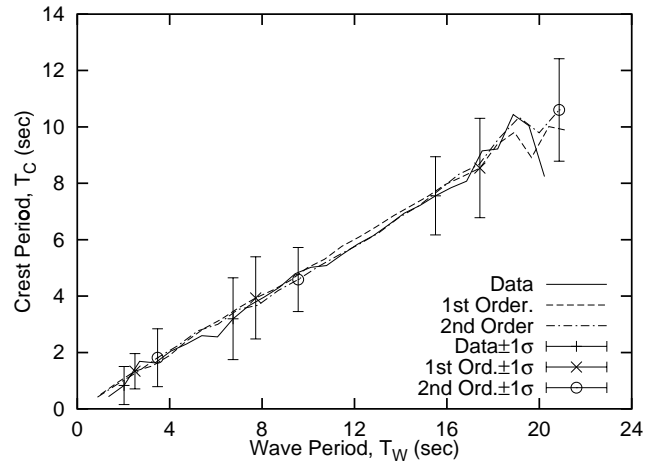


Figure 16. Crest Period T_C vs. wave period T_W

ods given crest heights for data, first- and second-order simulations. This figure shows the conditional median along with 16- and 84-percentile spread of wave periods given crest heights. All results show the same trend of increasing wave periods for small to moderate crest heights, and constant wave periods for large crest heights. The asymptotic wave period is close to the central period obtained from the first moment of the wave spectrum (in this case the central period is about 12 seconds; cf. Table 1). Figure 19 shows a similar comparison of conditional distribution of maximum of T_{CF} and T_{CB} in a wave vs. the crest height of the wave. This is again shown as the conditional median with 16- and 84-percentile scatter of $\text{Max.}(T_{CF}, T_{CB})$ given crest heights. Such statistics are of interest, for example, in identifying the large high-frequency resonant (“ringing”) responses that may be observed in offshore structures. Again, all results show the same trend of increasing periods for small crests and a gradual asymptote period for large crest heights, with the second-order model offering a slightly better agreement to data. The asymptotic maximum of the crest front and back period for large crest heights is about 25% of the central wave period.

CONCLUSIONS

This paper has addressed two distinct tasks: analytical models consistent with random second-order waves, and evaluation of these models with respect to observed wave behavior. Conclusions with respect to these tasks are as follows:

Analytical models of random second-order waves. A set of convenient analytical expressions has been shown to be consistent with the behavior of random second-order waves. These include useful approximations to (1) the wave skewness and kurtosis (from Eqns. 9–10), (2) the wave elevation CDF (Eqn. 12),

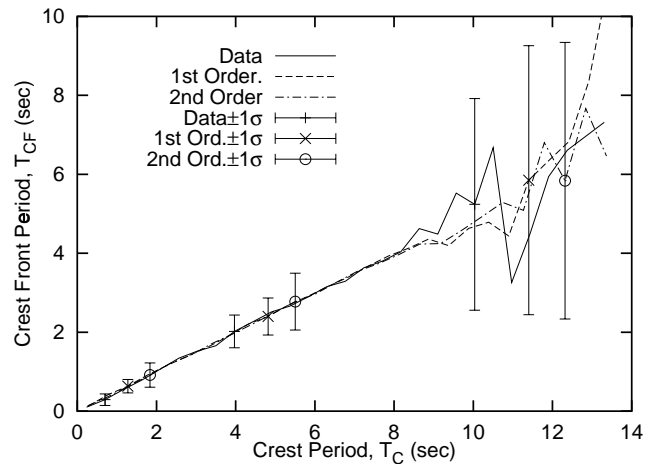


Figure 17. Crest front period T_{CF} vs. crest period T_C

(3) the wave crest CDF (Eqn. 14), and (4) the wave height CDF (Eqn. 16). Agreement of (2)–(4) is demonstrated here in Figures 3, 4, and 5 respectively. Hence we believe these analytical models accurately represent the behavior of second-order random waves. They remove the need for full time-domain simulation of second-order waves, involving double Fourier sums (e.g., Eqns. 4–5.)

Comparison of second-order models with wave data. The major finding is the notable difference between wave tank data (sets 1 and 2) and Ekofisk field data (set 3). This is most fundamentally seen at the wave moment level: while all data sets shows similar skewness levels, the wave tank data shows systematically greater kurtosis than the field data (Figures 1 vs 2). As these figures show, the second-order model accurately pre-

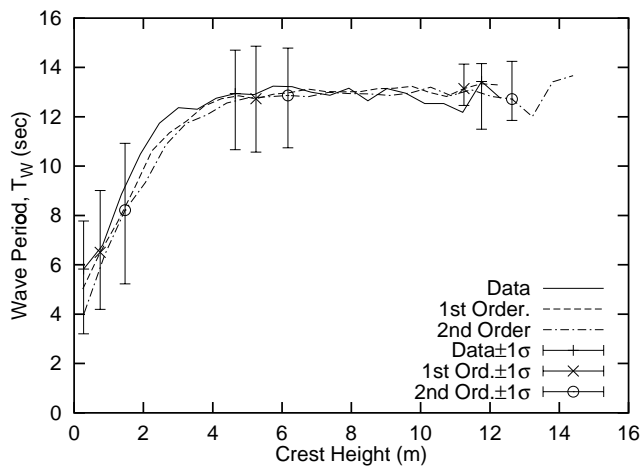


Figure 18. Wave period T_W vs. crest height

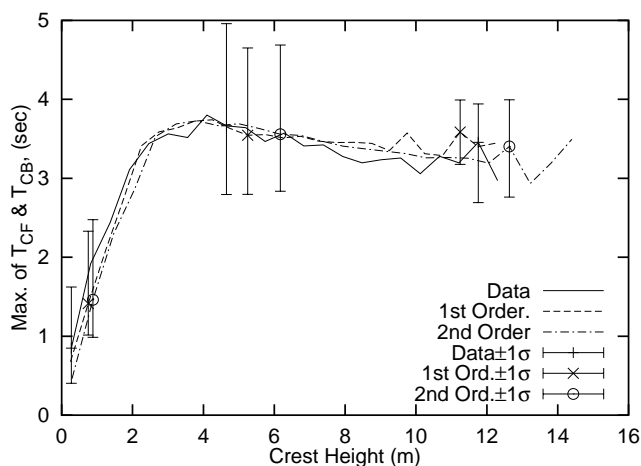


Figure 19. Maximum of crest front (T_{CF}) and crest back (T_{CB}) periods vs. crest height

dicts kurtosis trends for Ekofisk, but underestimates them for the wave tank histories. This discrepancy propagates through all CDF comparisons in a consistent manner: the analytical CDF models of wave elevations, wave crests, and wave heights accurately predict the Ekofisk results but somewhat underestimate wave tank results.

These differences between field data and model tests may be due to the higher severity of the model test seastates, and/or the possible short-crestedness of the field data. We caution also that our study of model tests here includes only two hours of data; however, preliminary study of other, longer wave tank histories appear to show similar trends. Should this prove to be the case, we recommend that the second-order models be enhanced

in some way—e.g., through empirical results that capture the enhanced kurtosis values as a function of wave steepness—to predict extreme wave levels. The Hermite model appears able to propagate these effects into the upper distribution tails, provided it is calibrated with accurate skewness and kurtosis values (as in the “Cubic Hermite” in Figure 6, which uses observed wave moments rather than those predicted by second-order theory).

ACKNOWLEDGMENTS

This study is part of the doctoral work of the first author and has been supported by the Office of Naval Research, grant N00014-95-1-0366, under the supervision of Dr. Peter Majumdar, and grant N00014-96-1-0641, under the supervision of Dr. Roshdy S. Barsoum. Additional funding has been provided by the Reliability of Marine Structures (RMS) program at Stanford University. The authors wish to thank Dr. Sverre Haver of Statoil for providing the North Sea wave data and Dr. Tom Marthinsen of Saga Petroleum for providing the wave tank data.

References

- Anastasiou, K., Tickell, R. G., & Chaplin, J. R. 1982. The nonlinear properties of random wave kinematics. *In: Proceedings of the 3rd International Conference on behavior of offshore structures*. MIT, Massachusetts.
- Forristall, G. Z. 1978. On the Statistical Distribution of Wave Heights in a Storm. *Journal of Geophysical Research*, **83**(C5), 2353–2358.
- Haring, R. E., Osborne, A. R., & L.-P., Spencer. 1976. Extreme Wave Parameters based on Continental Shelf Storm Wave Records. *Pages 151–170 of: Proceedings of the 15th Coastal Engineering Conference*.
- Hasselmann, K. 1962. On the non-linear energy transfer in a gravity-wave spectrum. *Journal of Fluid Mechanics*, 481–500.
- Hu, S.-L. J., & Zhao, D. 1993. Non-Gaussian Properties of Second-order Random Waves. *Journal of Engineering Mechanics*, **199**(2), 344–364.
- Huang, N. E., Long, S. R., Tung, C.-C., Yuan, Y., & Bliven, L. F. 1983. A Non-Gaussian Statistical Model for Surface Elevation of Nonlinear Random Wave Fields. *Journal of Geophysical Research*, **88**(C12), 7597–7606.
- Hudspeth, R. T., & Chen, M.-C. 1979. Digital simulation of nonlinear random waves. *Journal of the Waterway, Port, Coastal and Ocean Division*, **105**(WW1), 67–85.
- Jha, A. K., de Jong, P. R., & Winterstein, S. R. 1997. Motions of a spar buoy in random seas: Comparing predictions and model test results. *In: Proceedings, Behavior of Offshore Structures BOSS-97*. Delft Univ.

- Langley, R. S. 1987. A statistical analysis of non-linear random waves. *Ocean Engineering (Pergamon)*, **14**(5), 389–407.
- Longuet-Higgins, M. S. 1963. The effect of non-linearities on statistical distributions in the theory of sea waves. *Journal of Fluid Mechanics*, **17**(3), 459–480.
- MARINTEK. 1989. *TLP Hydrodynamic Model Tests*. Tech. rept. 511138.01. MARINTEK Trondheim, Norway.
- MARINTEK. 1990. *TLP Hydrodynamic Model Tests*. Tech. rept. 511217.01. MARINTEK Trondheim, Norway.
- Marthinsen, T., & Winterstein, S. R. 1992. On the skewness of random surface waves. *Pages 472–478 of: Proceedings of the 2nd International Offshore and Polar Engineering Conference, San Francisco*. ISOPE.
- Naess, A. 1985. On the Distribution of Crest to Trough Wave Heights. *Ocean Engineering*, **12**(3), 221–234.
- Schetzen, M. 1980. *The Volterra and Wiener Theories of Non-linear Systems*. New York: John Wiley & Sons.
- Sharma, J. N., & Dean, R. G. 1979 (July). *Development and evaluation of a procedure for simulating a random directional second order sea surface and associated wave forces*. Ph.D. thesis, University of Delaware.
- SWIM 2.0. 1995. *SWIM: Slow Wave-Induced Motions– User’s Manual*. Dept. of Ocean Engineering, M.I.T.
- Tayfun, M. A. 1980. Narrow-Band Nonlinear Sea Waves. *Journal of Geophysical Research*, **85**(C3), 1548–1552.
- Tick, L. J. 1959. A Non-linear Random Model of Gravity Waves I. *Journal of Mathematics and Mechanics*, **8**(5), 643–651.
- Ude, T.C., Jha, A.K., & S.R., Winterstein. 1993. *QTSTAT: Statistics of second-order systems. MAXMIN: Extremes of non-Gaussian processes*. Tech. rept. TN-1. Reliability of Marine Structures.
- Vinje, T., & Haver, S. 1994. On the Non-Gaussian Structure of Ocean Waves. *Pages 453–480 of: Proceedings of the 7th International Conference on the Behaviour of Offshore Structures (BOSS)*, vol. 2.
- WAMIT 4.0. 1995. *WAMIT: A Radiation-Diffraction Panel Program for Wave-Body Interactions–User’s Manual*. Dept. of Ocean Engineering, M.I.T.
- Winterstein, S. R., & Jha, A. K. 1995. Random models of second-order waves and local wave statistics. *Pages 1171–1174 of: Proceedings of the 10th Engineering Mechanics Speciality Conference*. ASCE.
- Winterstein, S. R., Bitner-Gregersen, E. M., & Ronold, K. O. 1991. Statistical and Physical Models of Nonlinear Random Waves. *Pages 23–31 of: OMAE - Volume II, Safety and Reliability*. ASME.
- Winterstein, S. R., Ude, T. C., & Kleiven, G. 1994a. Springing and Slow-Drift Responses: Predicted Extremes and Fatigue vs. Simulation. *Pages 1–15 of: Proceedings of the 7th International Conference on the Behaviour of Offshore Structures (BOSS)*, vol. 3.
- Winterstein, S. R., Ude, T. C., & Marthinsen, T. 1994b. Volterra Models of Ocean Structures: Extreme and Fatigue Reliability. *Journal of Engineering Mechanics, ASCE*, **120**(6), 1369–1385.